Dynamic Field Test of a Model Levee Founded on Peaty Organic Soil Using An Eccentric Mass Shaker

E.T. Reinert, S.J. Brandenberg & J.P. Stewart
University of California, Los Angeles

R.E.S. Moss
California Polytechnic State University, San Luis Obispo

SUMMARY:
A dynamic field test of a model levee was performed to study the behavior of very soft and compressible peaty organic soils that commonly underlie levees in the Sacramento / San Joaquin Delta in northern California. This first-of-its-kind test applied dynamic loads to the levee/peat system using a large eccentric mass shaker mounted on the levee crest. Loads from the shaker and the inertia of the levee section are transmitted to the peaty organic soils as base shear stresses, and rotational demands that manifest as normal pressures at the embankment/peat interface. We seek to characterize the transmission of seismic energy between the underlying soft peat and the overlying, comparatively stiff levee fills. A crucial step in the evaluation of the test data is calculation of the amplitude and phase of shaker forces. We compute the centrifugal force from discretely sampled proximity transducer data using a cosine sweep interpolation function.

Keywords: Levee, Peat, Eccentric Mass Shaker

1. INTRODUCTION

The seismic stability of levees in the Sacramento / San Joaquin Delta is critical to California's water distribution system (details in Lund et al. 2007, and DRMS 2009). The levees are composed of unengineered fills that are often sandy and susceptible to liquefaction, and typically rest atop peaty organic foundation soils, although liquefiable soils are also sometimes present in the foundations. Recent seismic hazard assessments indicate that liquefaction is the dominant source of potential earthquake-induced levee failures in the Delta (DRMS 2009). The liquefaction triggering potential of sandy soils is well understood, and this is unquestionably a serious problem for Delta levees. What is rather poorly understood at present is the manner by which the very soft, compressible non-liquefiable peat soils will transfer seismic energy into the overlying levees, and contribute to levee failure mechanisms. Case histories indicate that peat can play a role in levee failures (e.g., Sasaki 2009), but isolating the response of the peat is often difficult due to the presence of other poor soil conditions in these case histories.

To address the influence of peat on potential seismic levee deformation mechanisms, we performed forced vibration testing on a model levee constructed on free-field peat on Sherman Island using the NEES@UCLA MK-15 eccentric mass shaker. The study focused on the behavior of the underlying peat rather than the better-understood liquefaction behavior of loose sandy fills. The embankment was constructed from nonliquefiable unsaturated clayey fill reinforced with geogrids. The model levee was well-monitored using a combination accelerometers, pore pressure transducers, slope inclinometers, and string potentiometers. This paper focuses on calculation of the imposed shaker force from recorded proximity sensor and shaker base acceleration data. Computation of the shaker force is complicated by the uneven sampling interval at which rotation of the centrifugal mass is recorded, and by the translational component of acceleration mobilized when significant transient displacements are mobilized. Some sample data from the test program are also presented.

2. SITE INVESTIGATION

The model levee was constructed on a free-field site at Sherman Island on the western edge of the Delta. Our site investigation included hand augering with retrieval of samples using specially designed hand piston sampler, vane shear testing in the hand auger holes, visual classification, cone penetration testing with pore pressure and shear wave velocity measurements, and shear wave velocity measurements using SASW and ReMi. We also measured ambient vibrations at the site for the purpose of defining safe levels of vibration and for quantifying anticipated attenuation of wave energy with distance from the test specimen to quantify potential impacts of our shaking program on adjacent levees. Geophysical data are not presented herein for brevity. Measured shear wave velocities are below 30m/s.

Fig. 1 shows the results from the vane shear tests performed in the hand auger boreholes. The top 1.5m of soil consisted of stiff, unsaturated, fibrous peat. At 1.5m, the water table was encountered, and at 2m, the soil became so soft that the hand auger could be manually pushed downward into the peat without turning the cutting bit. Vane shear tests were performed primarily using a Geonor H60 hand-held device. Vane shear tests are typically performed slowly enough to accurately measure peak and residual undrained strengths during a single rotation. However, we were concerned that the high horizontal permeability of the peat would result in a partially drained response for a slow torque rate. Therefore, we rapidly torqued the vane, requiring only a few seconds to perform a test. Following measurement of the peak undrained shear strength, the vane torque gauge was re-set and the shearing was repeated to measure a residual undrained shear strength. Measured strengths and normalized shear strengths are plotted in Fig. 1. Peak undrained shear strength ratios in the saturated peat range from 0.28-1.17, while residual shear strengths range from 0.08-0.68

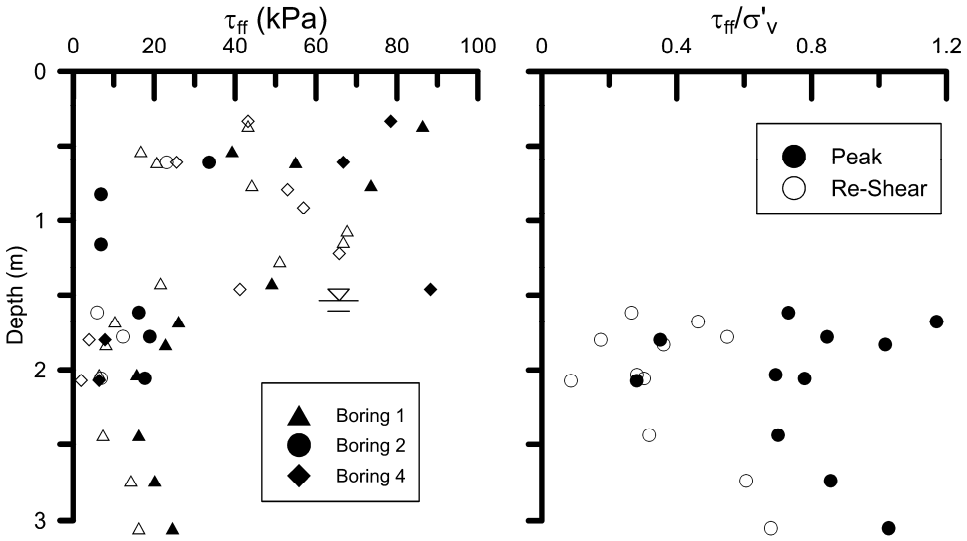

Figure 1. Vane shear test results.

Fig. 2 shows the CPT sounding logs obtained from the NEES@UCLA CPT rig. Tip resistance in the upper meter is zero because a hand auger hole was advanced and filled with water to prevent desaturation of the porous stone in the unsaturated upper layer. In the depth range from 2 and 11 meters, the cone experienced very little (at or below zero) tip resistance (q_t) and sleeve friction (f_s), indicating the presence of very soft peat in this interval. In fact, the peat was so weak in this interval that the project team had to physically hold up the cone and rod assembly with pipe wrenches when the clamp was released from the cone rods to prevent the rods from running under their own weight. To a depth of about 10.5 m, signal to noise ratios associated with the measured tip and sleeve resistances were small, and the soil behavior type (SBT) was therefore assigned based on independent

knowledge of the peat material rather than from cone measurements. Below 11m, the q_t and f_s increased dramatically, giving an SBT of silty sand/sandy silt for 11-16m depth on top of much stiffer sand and silty sand from 16-20m.

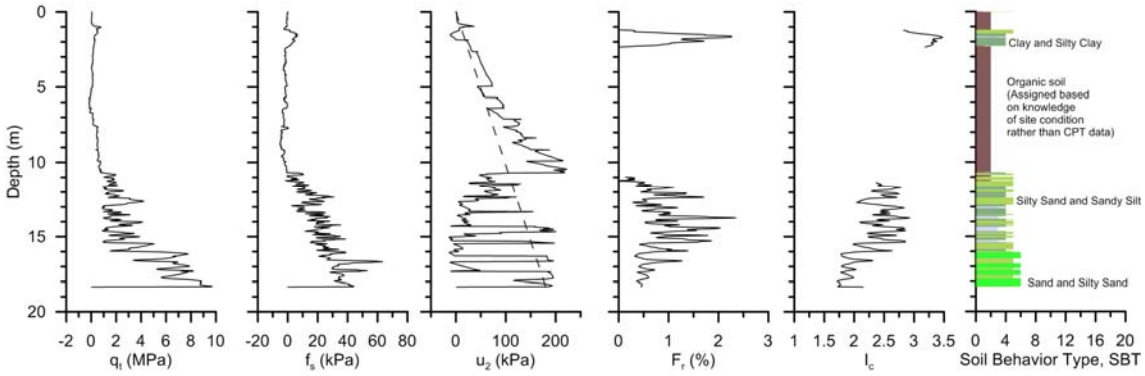

Figure 2. CPT results for Sherman Island site.

3. TEST SPECIMEN

The model test embankment consisted of a 1.8m (6ft) tall embankment with a 12.2m (40ft) long base, 4.9m (16ft) long crest with 2:1 sideslopes, and a 3.7m (12ft) out-of-plane width (Figs. 3 and 4). The embankment was constructed using compacted fill from a local borrow pit. Six lifts, each 0.3m (1ft) in height, were reinforced using a combination of biaxial geogrids and geosynthetics that were wrapped in the out-of-plane direction to form two vertical faces. A sturdy prefabricated timber frame designed to support the shaker was placed at the center of the embankment following compaction of the third lift. Soil was compacted around the timber frame to effectively provide 0.9m of embedment. A deck was subsequently attached to the top of the frame at the levee crest to support the shaker.

Prior to construction of the embankment, a horizontal inclinometer consisting of an array of MEMS accelerometers was laid horizontally on the ground surface to monitor settlement of the base of the embankment. Furthermore, the piezometers were inserted into the peat to monitor consolidation. A remote data acquisition system communicated settlement and pore pressure data to a website where consolidation was monitored remotely. Details of this instrumentation are beyond the scope of this paper. The subsurface accelerometers were installed after embankment construction, immediately prior to shaking, through PVC conduits that were left in the embankment.

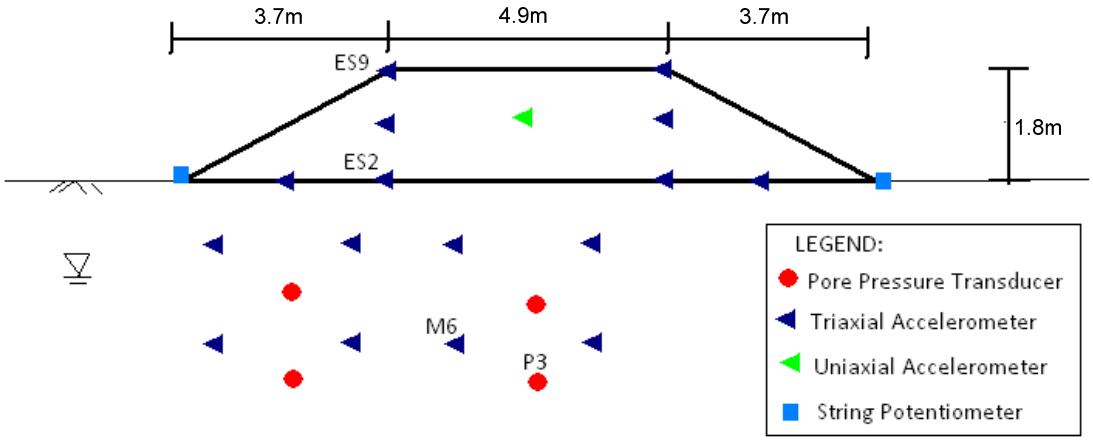

Figure 3. Embankment dimensions and instrumentation configuration (some sensors omitted for clarity).

Figure 4. Photograph of the completed embankment with mounted MK-15 shaker.

4. CALCULATION OF SHAKER FORCE

The force imposed by the eccentric mass shaker depends on the rotating mass, the angular frequency, the position of the baskets, and the acceleration of the base of the shaker in response to the imposed force. Eqn. 4.1 defines the shaker force in the +X direction (Fig. 1), where m_b is the non-rotating shaker mass, m_r is the rotating mass, $a_{b,x}$ is the acceleration of the shaker base in the +X direction, r is the radius from the center of rotation to the centroid of the rotating mass, ω is the angular frequency, and θ is the position of the rotating mass.

$$F_x = \left(m_b + m_r\right) a_{b,x} + m_r r \omega^2 \cos\theta \tag{4.1}$$

The position of the rotating masses is recorded using two proximity sensors that measure the passage of steel pins mounted on circular plates affixed near the pivots (Fig. 1b). One plate contains ten pins evenly distributed around the circumference of the steel plate for the purpose of accurately measuring ω, and the other plate contains a single pin for the purpose of accurately measuring θ. As each pin passes within range of the proximity sensor, the recorded voltage jumps from 0 to 10 VDC, thereby producing a sequence of pulses. The plate with a single pin is configured such that the rotating masses are aligned in the +X direction when the center of the pulse occurs. The plate with 10 pins is ill equipped for measuring position because the recorded pulses cannot be mapped to individual pin positions. However, this plate provides a means for accurately computing angular frequency by measuring the time that elapses between pulses.

The data for the proximity sensors are recorded uisng a National Instruments data acquisition system with a sampling frequency of 2000 Hz. The National Instruments system is manually triggered to begin recording a few seconds before the command is sent to commence rotation of the shaker baskets. A different data acquisition system is used to continuously record data from the accelerometers, pore pressure transducers, and string potentiometers, and the National Instruments data is therefore not time-synchronized with the other recorded quantities. Co-located accelerometers, one recorded by the National Instruments system, and the other recorded by the other system, are used to synchronize the data from the two different systems. Frequency-domain cross-correlation of the records from the co-located accelerometers is used to align the shaker force function with the other recorded data.

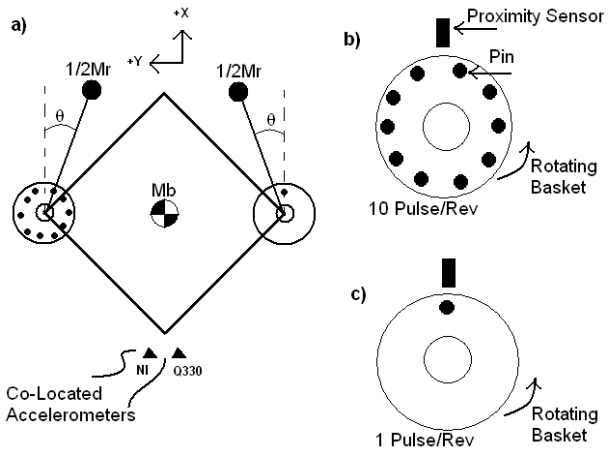

Figure 5. MK-15 eccentric mass shaker instrumentation detail.

Fig. 6 shows example data recorded from the proximity sensors during one of the shake tests. The voltage from the proximity sensor for the plate with 10 pins begins at 10 V, which indicates that the shaker was initially oriented such that one of the pins was within range of the proximity sensor. The voltage subsequently drops to zero as the pin passes out of range, and then rapidly increases to ten volts again as the next pin moves into range. The duration of the pulses decreases with time as the angular frequency increases. The pulses recorded for the plate with a single pin indicate times when the baskets are oriented in the +X direction.

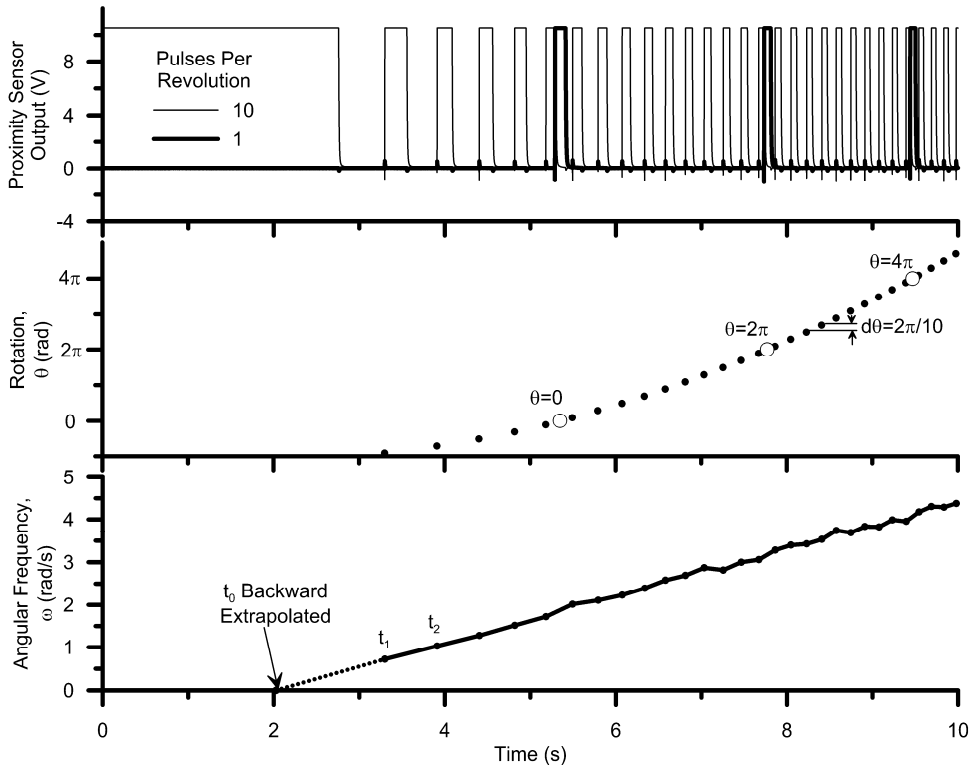

Figure 6. Pulses recorded from proximity sensors, and computed rotation and angular frequency.

Fig. 6 also shows rotation angle versus time computed from the proximity sensor data. The incremental rotation corresponding to each pulse recorded for the plate with 10 pins is equal to $2\pi/10$. A constant is subsequently subtracted from the computed rotation angle so that θ is zero at the time when the center of the first pulse is recorded for the plate with a single pin. Angular frequency is

computed from the rotation angle data using numerical differentiation defined by the backward Euler equation $\omega_i=(\theta_i-\theta_{i-1})/(t_i-t_{i-1})$. Note that the time when the shaker begins moving is not known, and is backward extrapolated by linear interpolation of angular frequency versus time.

The recorded proximity sensor data have now been converted into time series of θ and ω discretized into uneven time intervals corresponding to 10 data points per cycle, and the shaker force can be computed at these same unevenly sampled time intervals. However, we desire to compute the shaker force at different time intervals corresponding to the acceleration, pore pressure, and displacement data sampled at a constant frequency of 200 Hz. The simplest method involves linear interpolation of the shaker forcing function at the discrete times when samples were recorded for the other sensors. The problem with this method is that the shaker force is not anticipated to vary linearly in time; rather, it is the angular frequency that is anticipated to vary linearly in time in accordance with the command function. For this reason, a more complex cosine sweep function is utilized. The general form of the cosine sweep function is given in Eqn. 4.2. Represented in discrete form in Eqn. 4.3, the shaker force, $F_{x,k}$, interpolated at a particular time t_k, where the index i indicates the unevenly sampled rotation data, index k indicates the discrete times at which shaker forces are desired to be evaluated (so that they correspond to other recorded quantities), ω_k is linearly interpolated at t_k from the unevenly sampled ω vector, and θ_0 is the initial angle of the baskets when the shaker first began rotating (i.e., the constant of integration from Eqn. 4.2.

$$Sweep(t) = \cos\left(\int_0^t \omega(t')dt'\right) \tag{4.2}$$

$$F_{x,k} = m_r\omega_k^{\,2}\cdot\cos\left(\sum_{i=1}^{k}\left(\theta_i-\theta_{i-1}\right)+\theta_0\right)+\left(m_r+m_b\right)a_{b,x} \tag{4.3}$$

Fig. 7 shows the shaker force data recorded at uneven sampling intervals, along with the results from linear interpolation and cosine sweep interpolation. The cosine sweep interpolation provides superior data quality by preserving the smoothly varying frequency content of the command input to the shaker. Furthermore, the amplitude of the shaker force is 4% higher using the cosine interpolation method compared with the linear interpolation method because the irregularly sampled rotation data do not happen to correspond to a peak in the shaker forcing function. Although modest, this difference is not negligible and may be important for certain applications that are sensitive to the shaker force. The shaker forcing function is then aligned with the other recorded data using cross-correlation between the co-located accelerometers on the shaker base. A phase error of 1 or 2 data points may arise from this cross-correlation procedure, which could influence computed damping values.

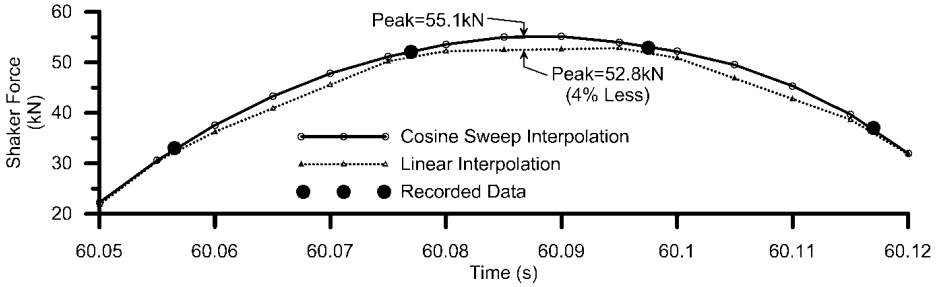

Figure 7. Shaker force interpolated using linear interpolation, and cosine sweep interpolation for a portion of one cycle.

Acceleration of the shaker base influences the force imposed by the shaker by introducing a translational component of motion in addition to the rotational component. The influence of translation on the shaker force is a function of the displacement of the center of rotation of the rotating mass relative to the radius of the rotating mass. Fig. 8 shows shaker base acceleration and shaker force

computed with and without the translational component for two motions; one small and one large. For the small motion, the translational component of motion has very little influence on the imposed shaker force. However, the large motion induced significant movement of the shaker base as a result of formation of a gap between the timber frame and the compacted clay fill, resulting in an irregular acceleration record. Failure to account for the translational component (i.e., by computing shaker force only as $m_r r\omega^2 \cos\theta$) resulted in a 6.8% over-prediction of shaker force in this case. This case illustrates the importance of accounting for translational motion in the calculation of shaker force for cases where significant transient displacements are mobilized.

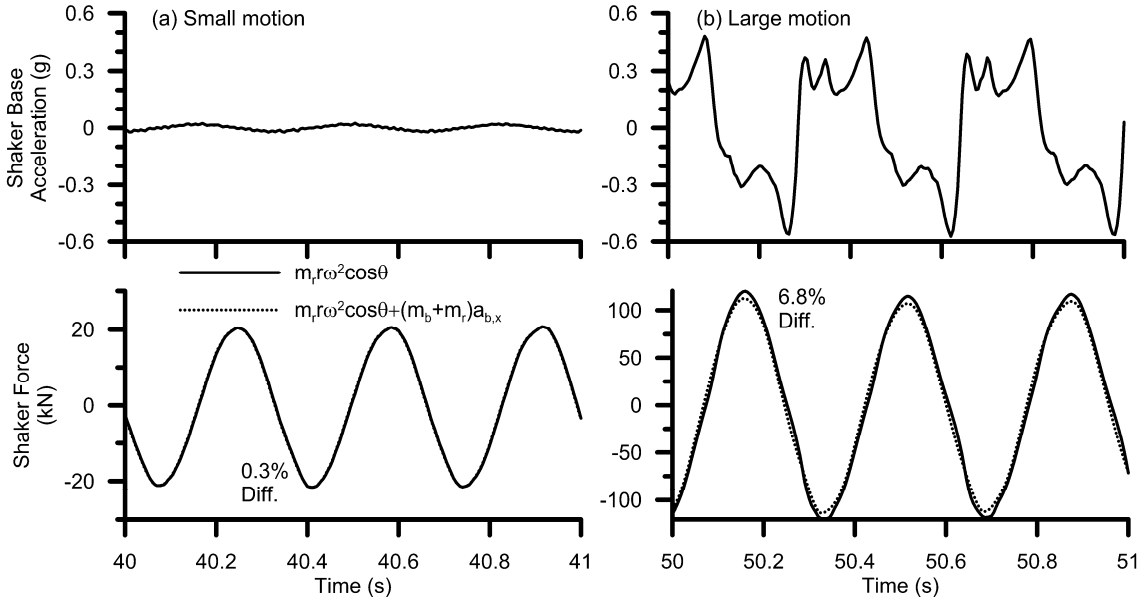

Figure 8. Shaker base acceleration and corrected/uncorrected shaker force functions for (a) a small motion (MK15_1_4) and (b) a large motion (MK15_4_1).

5. SAMPLE TEST DATA

Fig. 9 shows the horizontal acceleration in the direction of shaking at the top of the embankment, bottom of the embankment, and at a depth of 3m (9ft) in the peat for a 10 second excerpt one of the small shaking events (the entire event lasted 120s). The recorded motion was largest at the top of the embankment (0.085g max) and smallest in the peat (0.021g max). The peak acceleration at the embankment crest is more than double the peak acceleration of the embankment base (0.036g max), which is likely due to a combination of embankment rocking and topographic amplification. Further reduction of ground motions deeper in the peat are likely caused by a combination of geometric spreading of seismic waves and material damping.

Fig. 10 shows the development of pore water pressure at 4m (12 ft) beneath the center of the embankment for one of the strong shakes. During shaking, dynamic pore pressure changes are observed. After shaking, pore pressures continued to increase. The cause of the continued increase in pore pressure after shaking is currently unclear. A common cause of delayed pore pressure response is unsaturation in the pore pressure sensor. However, good quality dynamic pore pressures were measured during shaking, which indicates the piezometer was well saturated. The cause of this behaviour is currently being investigated in laboratory studies of the post-cyclic consolidation behavior of peat. Overall, the increase in pore pressure from the shake is only 0.35 kPa, which is small compared to the initial vertical effective stress.

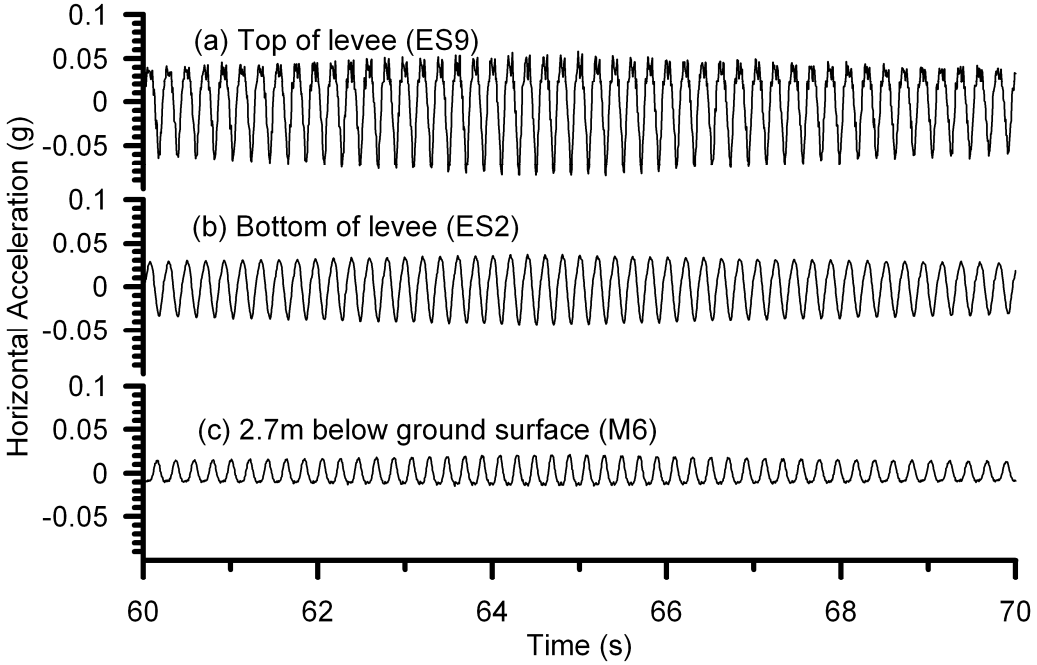

Figure 9. Acceleration versus depth for a small shake.

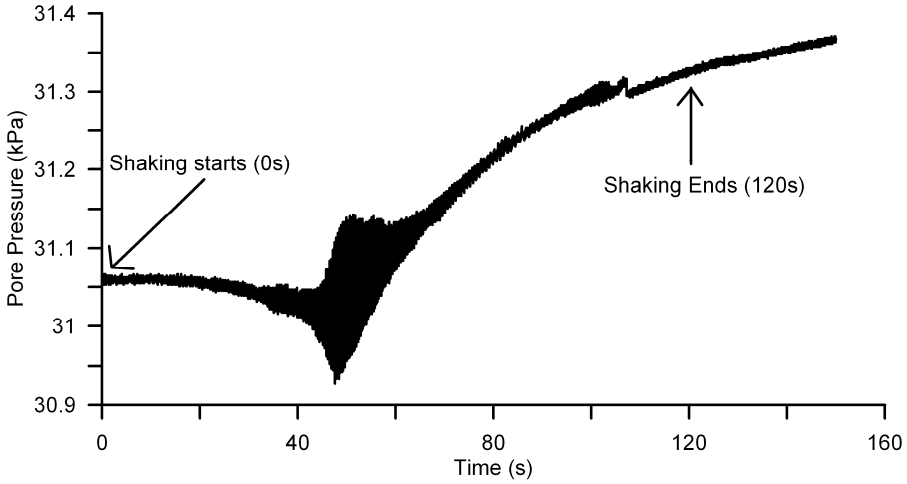

Figure 10. Pore water pressure recorded at a depth of 4m.

6. CONCLUSIONS

A field test of a model levee founded on peaty organic soil was performed using an eccentric mass shaker mounted to the levee crest. The focus of this paper is calculation of the force imposed at the base of the eccentric mass shaker from the proximity sensor data used to define the position of the rotating baskets. Two significant effects that could easily be erroneously excluded from calculation of shaker force were explored in this paper. First, a cosine sweep interpolation function provided superior results with respect to amplitude and frequency content compared with the simpler linear interpolation method because the linear variation of frequency with time is preserved using cosine sweep interpolation. Second, translational acceleration of the shaker base can cause the shaker forcing function to differ moderately from $m_r r\omega^2 \cos\theta$ when the imposed demands cause significant transient displacements of the test specimen. The effect was observed to be small for a small input motion, but as high as 6.8% for a large input motion for the test sequence presented herein. This non-negligible

effect should therefore be considered when interpreting eccentric mass shaker data.

Sample data show that: (1) significant ground motions were imposed at the levee crest, (2) ground motion intensity was stronger at the center of the levee crest than at the center of the levee base, which is consistent with the observation of significant rocking of the model embankment, and (3) mobilization of excess pore pressures was very small. A relatively stiff unsaturated layer of peat atop the softer saturated peat may have shielded the saturated peat from significant ground motion. Additional testing will be needed to evaluate this effect.

AKCNOWLEDGMENTS

The authors would like to acknowledge the following people for assistance during the test: Mike Driller and Bryan Brock from the Department of Water Resources, the nees@UCLA group including Bob Nigbor, Steve Keowen, Alberto Salamanca, Sophia Poulos and Jackson English, and UCLA students Pavlo Chrysovergis and Ali Shafiee. This research was supported by the National Science Foundation under award number 0830081 through the George E. Brown Network for Earthquake Engineering Simulation Research (NEESR) program in coordination with cognizant program official for this grant is Richard J. Fragaszy. Any opinions, findings, and conclusions or recommendations expressed in this material are those of the author(s) and do not necessarily reflect the views of the National Science Foundation. This material is based upon research performed in a renovated collaboratory by the National Science Foundation under Grant No. 0963183, which is an award funded under the American Recovery and Reinvestment Act of 2009 (ARRA).

REFERENCES

Lund, J., E. Hanak, W. Fleenor, R. Howitt, J. Mount, and P. Moyle, (2007). "Envisioning Futures for the Sacramento–San Joaquin Delta." Public Policy Institute of California, San Francisco, California.

Sasaki, Y. (2009). "River dike failures during the 1993 Kushiro-oki earthquake and the 2003 Tokachi-oki earthquake," Earthquake geotechnical case histories for performance-based design - Kokusho (ed), 2009 Taylor & Francis Group, London, pp. 131-157, 2009.

URS Corporation, Jack R. Benjamin and Associates (2009). "Delta Risk Management Strategy (DRMS) Phase 1 Report." California Department of Water Resources.

Wehling, T., R. Boulanger, et al. "Nonlinear Dynamic Properties of a Fibrous Organic Soil." Journal of Geotechnical and Geoenvironmental Engineering. 129.10 (2003): 929-39.